

The direct assembly of Mg–Al LDH nanosheets and Mn(II)–salen complex into sandwich-structured materials and their enhanced catalytic properties†

Cite this: *RSC Adv.*, 2013, **3**, 19885

Received 8th June 2013
Accepted 16th August 2013

DOI: 10.1039/c3ra42837k

www.rsc.org/advances

Liyan Dai,* Jing Zhang, Xiaozhong Wang and Yingqi Chen

The direct assembly of LDH nanosheets and organic molecules, such as Mn(II)–salen complex, into a sandwich-structured nanocomposite has been achieved *via* a modified flocculation method. When used as a catalyst, the obtained material has superior thermal stability and catalytic properties over a material prepared using a traditional ion exchange method in the oxidation of 4-picoline.

The preparation of clay mineral particles on the nanoscale is an active area of academic and, more importantly, application research in the fields of electronics, photonics, magnetism and catalysis.¹ In particular, LDHs (layered double hydroxides, $[M^{2+}_{1-x}M^{3+}_x(OH)_2][A^{n-}]_{x/n} \cdot zH_2O$) that consist of stacks of positively charged metal hydroxide layers and exchangeable interlayer anions have been extensively studied, particularly their delamination processes.² The resulting nanosheets can be used as flexible building blocks to create novel organic–inorganic or inorganic–inorganic nanomaterials. Different forms of LDH nanocomplex have been developed as catalysts, using electrostatic sequential deposition, flocculation or layer-by-layer (LBL) methods over the last few years.³ Among these methods, flocculation is the most convenient and provides a rational way to design novel materials with controlled nanostructures.⁴ Using a flocculation process, target species can be easily and rapidly loaded into the nanocomposite materials. As reported, inorganic nano-colloids such as AuNPs⁵ and oxide nanosheets⁶ have been assembled with LDH nanosheets *via* spontaneous flocculation, forming sandwich-structured materials. However, the arrangement is different when organic macromolecules are involved. Anionic porphyrins, first reported by Nakagaki and coworkers,⁷ were simply adsorbed on to the surface of LDH crystals instead of intercalating into the interlayers of the LDHs

via flocculation. If all of the organic particles were exposed on the surface of the solid, it would reduce the stability of the materials and make only limited use of the native structural properties of LDHs. Currently, most reports have been concerned with the intercalation chemistry of LDHs using ion exchange methods and stepwise LBL,⁸ however, the direct assembly of LDH nanosheets and ionic organic particles has still not been achieved. In contrast, this method is so intriguing because not only is the interlayer of the LDH completely open, resulting in no steric hindrance for the immobilization of macromolecules, but it also avoids the complex operations of other processes. In this regard, it is desirable to modify existing flocculation methods to intercalate organic molecules into LDH nanosheet galleries. This process will definitely provide a much simpler and more widely applicable strategy for material syntheses.

In this work, we have reported the direct combination of LDH nanosheets and an ionic Mn(II)–salen complex to form a nano-sized sandwich-structured material for the first time and then explored its catalytic properties. In order to prepare a suspension of LDH nanosheets, a new way to exfoliate LDH was developed that incorporated benzoate. The well-established nanosheets were combined with an ionic Mn(II)–salen complex through a modified flocculation process yielding ordered sandwich-structured particles. We then applied the obtained materials to the N-oxidation of pyridines, which resulted in enhanced catalytic properties over a material prepared using a traditional ion exchange method and its homogeneous analogue.

The LDH incorporated with benzoate (LDH-BA) was synthesized according to a coprecipitation method from the literature⁹ and then delaminated in formamide to obtain a stable and transparent colloid suspension using an ultrasonic treatment. Dispersions of LDH-BA were prepared with concentrations of 10 g L⁻¹, 20 g L⁻¹, 30 g L⁻¹ and 40 g L⁻¹ using an ultrasonic treatment (see Scheme S1†). Gelation happened at high concentrations (30 g L⁻¹ and 40 g L⁻¹) after resting for few days. However, the transparent and colourless sol of the lower

Department of Chemical and Biological Engineering, Zhejiang University, Hangzhou, P.R. China. E-mail: dailiyan@zju.edu.cn; Fax: +86-571-87952693; Tel: +86-571-87952693

† Electronic supplementary information (ESI) available. See DOI: 10.1039/c3ra42837k

concentration dispersions (10 g L^{-1}) could be maintained, even for months. The delamination process was further investigated using the LDH-BA dispersion with a concentration of 10 g L^{-1} . As illustrated in Fig. S1a,† a clear Tyndall effect can be observed, which provides evidence for the formation of exfoliated LDH-BA nanosheets. Disk-like particles were seen using TEM with particle sizes ranging from 20 nm to 100 nm (Fig. S2b†). Zeta potential measurements demonstrated that the LDH-BA nanosheets were in positively charged state (Fig. S1c†). The average particle size is $\sim 100 \text{ nm}$, which can be further characterised using DLS measurements (see Fig. S1d†). The AFM analysis, shown in Fig. S1e,† further confirmed that LDH-BA delaminated into single sheets. The height measurement curves show that the completely delaminated LDH nanosheets possess a height of $\sim 0.7 \text{ nm}$ (see the green curve), while some particles are thicker, with heights of up to $\sim 2 \text{ nm}$ (see the red and blue curves).

The preparation of Cat.1 was conducted by exchanging BA with an anionic salen complex at rt as reported in the literature.¹⁰ Cat.2 was prepared by adding exfoliated LDH-BA nanosheets, at a speed of 0.1 mL min^{-1} , into a salen-water solution at a high stirring speed. A slow feeding rate and fast stirring speed are key to controlling the crystal size of the nanoparticles. Restacking of the LDH nanosheets occurred as soon as they came into contact with the salen-water solution. Formamide molecules were replaced with H_2O and the ionic salen complex acted as a bridge, combining the separate nanosheets layers together to form the sandwich-structured Cat.2. Elemental analysis (C, H and N) and ICP-AES clearly demonstrated that the specific formula of LDH-BA is $\text{Mg}_{0.66}\text{Al}_{0.32}(\text{OH})_2(\text{BA})_{0.3} \cdot \text{H}_2\text{O}$, and the weight percentages of salen complex in Cat.1 and Cat.2 were 18.3 and 20.1 wt%, respectively (see Table S1†).

The XRD patterns of LDH-BA, Cat.1 and Cat.2 are shown in Fig. 1. All of the present samples possessed the same reflection (010) in the high 2θ region, indicating that the Mg/Al ratio was unchanged and the characteristic LDH structure was well maintained after the ionic exchange (Cat.1) or restacking process (Cat.2). A basal spacing of 15.2 \AA for LDH-BA was calculated from the (003) reflection, which corresponds to the formation of a benzoate bilayer-like structure within the gallery.^{11,12} Given that the hydrophobic groups stay in the middle of the layer much like fatty acids, it is easy for delamination to occur in a polar solvent. The (003) reflection is retained in Cat.1, although its intensity is decreased and several overlapped reflections appear in the low 2θ region, indicating that LDH-BA is partly intercalated with the salen complex. The basal spacings of the two main reflections (*) are 18.9 \AA and 31.5 \AA , suggesting that the arrangement of the salen and BA layers is regular (see Scheme S2†). Notably, a new reflection at 3.5° , which is characteristic of Cat.2, confirmed the successful intercalation of the salen complex into the interlayer of LDH. The d -spacing was 24.5 \AA , which is larger than the salen-layer in Cat.1 (18.9 \AA) and the previously reported value (18.78 \AA).¹³ The calculated size of the Mn(II)-salen complex is $17\text{--}18 \text{ \AA}$. The salen complex in Cat.1 might be oriented diagonally at an angle less than 90° to the layers,¹⁴ while it is perpendicular in Cat.2 as the layers of LDH-BA were totally

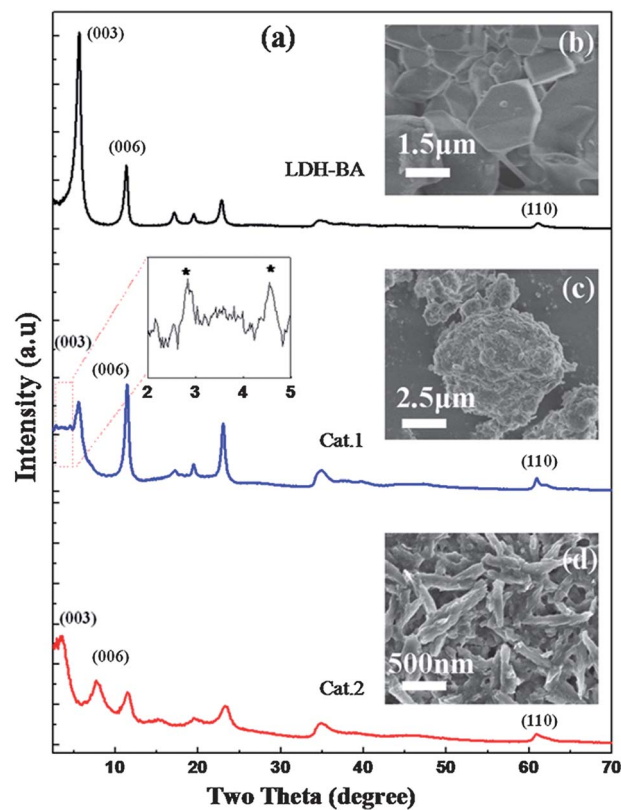


Fig. 1 (a) XRD patterns of LDH-BA, Cat.1 and Cat.2. SEM images of (b) LDH-BA, (c) Cat.1 and (d) Cat.2.

opened up *via* delamination and no barrier existed for the intercalation of the salen complex. Interestingly, adding the salen complex solution dropwise into the LDH-BA nanosheet suspension as in the literature,⁷ results in the anionic salen molecules being simply adsorbed on to the surfaces of the LDH crystals (see Fig. S2†). No reflections appeared in the low 2θ region ($<10^\circ$), confirming that: (1) BA molecules were fully dissolved in the formamide solution during delamination and (2) no salen molecules were inserted into the interlayers after restacking. Therefore, the results of XRD determined that our modified flocculation process was effective, providing Cat.2 with a clear sandwich-structure. SEM images of LDH-BA, Cat.1 and Cat.2 are shown in Fig. 1. Hexagonal platelets of LDH with a typical size of $3 \mu\text{m}$ were observed. After ion exchange, Cat.1 features a much larger particle size and more agglomeration than LDH-BA. For Cat.2, regular rod-like particles with a micrometer long and a nanometer wide were formed as expected. FT-IR spectra of the obtained samples are shown in Fig. S3.† The profiles of curves c and d are nearly identical, indicating that the compositions of Cat.1 and Cat.2 are similar. The imine $\text{C}=\text{N}$ stretching vibration of the free ligand at 1623 cm^{-1} shifts to 1640 cm^{-1} for Cat.1 and 1633 cm^{-1} for Cat.2. The bands at 1115 and 1032 cm^{-1} , corresponding to the sulfonato groups further confirm the successful intercalation of the anionic salen complex.

The thermal stabilities of LDH, Cat.1 and Cat.2 were studied using simultaneous thermal analysis (TGA-DTA) under a N_2

atmosphere. Fig. S4(a)† shows a total weight loss of up to ~48 wt % and ~44 wt% for LDH and Cat.1 and Cat.2, respectively, at 700 °C, which could be due to the loaded salen complex. For instance, in order to reach the same decomposition level of 25%, the required temperature increased from 350 °C for LDH-BA to 380 °C for Cat.1 and to 515 °C for Cat.2. Obviously, the thermal stability of Cat.2, which was prepared after rebuilding the LDH nanosheets, is far better than that of Cat.1, prepared using the traditional ion exchange method. The exothermic and endothermic conditions are other important pieces of evidence related to crystallization and decomposition, which can be detected using DTA. As shown in Fig. S4(b),† the first endothermic peaks for all three samples are observed at ~70 °C and can be attributed to the elimination of water molecules including physisorbed and crystallized water.¹⁵ However, the second endothermic peak, associated with layer dehydroxylation and interlayer anion decomposition, appears at different positions: the ion exchange of benzoate with salen complex improves the alignment of the crystal resulting in a 40 °C increase, while after assembly of the LDH nanosheets the crystal alignment is even better, which is in agreement with the results of TGA. Thus, the excellent thermal stability of Cat.2 can expand its application to different oxidation reactions with broad temperature requirements.

Since Mn(II)-salen complexes are well known for their efficient reactivity in oxygenation reactions, we decided to apply our catalyst to the N-oxidation of pyridines, which is the first example of applying a Mn(II)-salen complex in this oxidation. High temperature (90 °C) and acidic conditions are always required to obtain N-oxides of pyridines during industrial production, however our catalyst was able to provide an efficient and mild route, facilitating the oxidation of pyridines at room temperature. The catalytic performance of Cat.1, Cat.2 and the mono complex was investigated using 30% H₂O₂ or molecular oxygen as the oxidant in water, with 4-picoline used as the raw material (Scheme 1). As can be seen in Table 1, when obtaining the target N-oxide of 4-picoline using 30% H₂O₂ (entry 1, 3, 5), Cat.2 displayed superior activity over the other catalysts, including Cat.1 and their homogeneous analogue. The catalyst turnover frequency of Cat.2 was the highest, showing 2–10 fold activity over the others. Blank experiments demonstrated that with LDH (entry 7) or only the oxidant (30% H₂O₂, entry 8) in the system the reaction did not proceed. We believe that the structural properties of LDH are responsible for the enhancement of the catalytic performance (Cat.1 and 2). LDHs are weak bases and can help to cleave the peroxide bond in H₂O₂ due to the formation of H-bonding between the OH⁻ of LDH and a hydrogen atom of H₂O₂. Therefore, the capacity of H₂O₂ was improved. A comparison between Cat.1 and Cat.2 also reveals that the size of the nanoparticles of Cat.2, not only increases the

Table 1 The N-oxidation of 4-picoline using Cat.1, Cat.2 and their homogeneous analogue^a

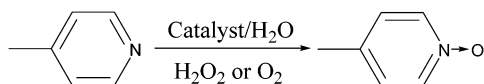
Entry	Catalyst	Oxidant	Time/h	Yield ^b (%)	TOF ^c
1	Mono-salen	H ₂ O ₂	5	77	42
2	Mono-salen	O ₂	24	56	6.2
3	Cat.1	H ₂ O ₂	8	84 (83) ^d	176
4	Cat.1	O ₂	24	—	—
5	Cat.2	H ₂ O ₂	3.5	95 (93) ^d	415
6	Cat.2	O ₂	24	22	14
7	LDH	H ₂ O ₂	24	—	—
8	—	H ₂ O ₂	24	—	—

^a All reactions were carried out using 10 mmol 4-picoline and 20 mg catalyst in 20 mL DD water with 0.68 g (30 mmol) H₂O₂ or molecular oxygen at room temperature. ^b The yield was determined using HPLC. ^c TOF (turnover frequency) = mmol of product per mmol of catalyst per hour. ^d Product yields after 6 recycles.

specific surface area, but also remarkably decreases the diffusion distance for the substrate from the reaction system to the active site in the material due to its nanoscale thickness. However, the catalytic results were very different when molecular oxygen was used as the oxidant (entry 2, 4, 6). The reaction rate decreased rapidly and the yields were not good, even after 24 hours for all of the catalysts. In addition, the homogeneous analogue, contrary to the previous results, showed higher catalytic activity than Cat.1 and Cat.2. This might be due to the poor solubility of molecular oxygen in water, which inhibits its combination with the active center in the interlayer of the LDH. Furthermore, solvent effects have also been discussed, which show that water is the best solvent for this reaction, while the yield is poor in other solvents such as methanol, ethanol, acetonitrile and dichloromethane (see Table S2†). The recyclability of Cat.1 and Cat.2 was tested under the same conditions. The results demonstrated that both heterogeneous catalysts were stable for 6 cycles with a slight loss of catalytic activity. The high stability of Cat.2 over these cycles is mainly due to the strong electrostatic interaction between the negatively charged Mn(II)-salen complex and the positively charged LDH nanosheet layers.

To further investigate the stability of our catalyst, further tests have been conducted. Electron spin resonance (ESR) spectra of Cat.2 and Cat.2' (after 6 recycles) are shown in Fig. 2. As can be seen, the typical six hyperfine splitting lines were well resolved around $g = 2.0$, corresponding to the hyperfine coupling of the low spin state ($S = 1/2$) of the Mn²⁺ ion's electronic spin with its 5/2 nuclear spin.¹⁶ After being recycled 6 times in the reaction, the intensity decreased a little, but there is no change in the hyperfine splittings of the six-line pattern. This result confirms that the Mn(II) species remains the same after oxidation. The result of ICP-AES analysis showed no trace of Mn in the filtrate, inferring that no demetallation occurred. The main reason for the yield decrease might be contamination of the active center by the substrate.

In conclusion, we report the delamination of LDH and incorporation of benzoate in formamide. In addition, we have demonstrated the successful direct assembly of LDH and



Scheme 1 The oxidation of 4-picoline to give its N-oxide.

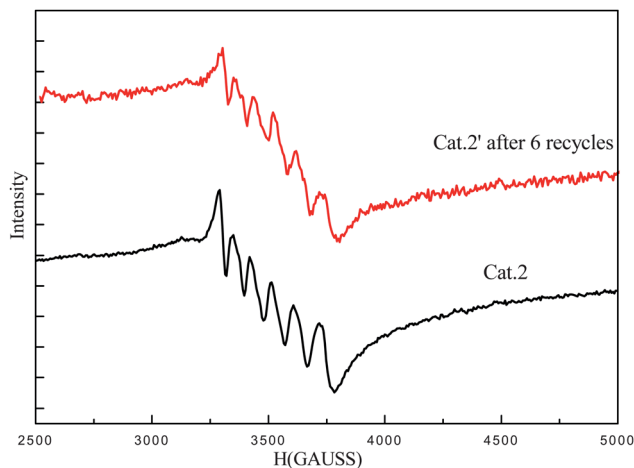


Fig. 2 ESR spectra (9.85 GHz, room temperature, microwave power: 102 mW) of Cat.2 and Cat.2' (after 6 recycles).

Mn(II)-salen complex using a modified flocculation process, thus providing a practical solution to introduce organic molecules into LDH galleries. The particles, when used as catalysts, showed remarkable catalytic properties and thermal stability over that prepared using a traditional ion exchange process. The yield of the oxidation of 4-picoline to its *N*-oxide was over 90%, even after the catalyst was recycled 6 times. The reaction was both green and low cost, and the preparation was simple, thus offering an effective strategy for industrial production.

This work was supported by the NSFC (no: 21176213), and Zhejiang Key Innovation Team of Green Pharmaceutical Technology (no: 2010R50043).

Notes and references

- 1 Y. Wang, W. S. Yang and J. J. Yang, *Electrochem. Solid-State Lett.*, 2007, **10**, A233–A236; J. Zhao, X. Kong, W. Shi, M. Shao, J. Han, M. Wei, D. G. Evans and X. Duan, *J. Mater. Chem.*, 2011, **21**, 13926; L. Li, Y. J. Feng, Y. S. Li, W. R. Zhao and J. L. Shi, *Angew. Chem., Int. Ed.*, 2009, **48**, 5888–5892; J. Z. Wang, L. W. Zhao, H. M. Shi and J. He, *Angew. Chem., Int. Ed.*, 2011, **50**, 9171–9176.
- 2 R. Ma, Z. Liu, L. Li, N. Iyi and T. Sasaki, *J. Mater. Chem.*, 2006, **16**, 3809; Q. Wang and D. O'Hare, *Chem. Rev.*, 2012, **112**, 4124–4155.
- 3 F. Wypych, G. A. Bubniak, M. Halma and S. Nakagaki, *J. Colloid Interface Sci.*, 2003, **264**, 203–207; A. N. Ay, N. V. Abramova, D. Konuk, O. L. Lependina, V. I. Sokolov and B. Zümreoglu-Karan, *Inorg. Chem. Commun.*, 2013, **27**, 64–68; D. Yan, J. Lu, J. Ma, M. Wei, D. G. Evans and X. Duan, *Angew. Chem., Int. Ed.*, 2011, **50**, 720–723; M.-Q. Zhao, Q. Zhang, J.-Q. Huang and F. Wei, *Adv. Funct. Mater.*, 2012, **22**, 675–694; S. He, Z. An, M. Wei, D. G. Evans and X. Duan, *Chem. Commun.*, 2013, **49**, 5912; A. Zhe, H. Jing and D. Xue, *Chin. J. Catal.*, 2013, **34**, 225–234.
- 4 L. Li, R. Ma, Y. Ebina, K. Fukuda, K. Takada and T. Sasaki, *J. Am. Chem. Soc.*, 2007, **129**, 8000–8007.
- 5 L. Li, Q. Chen, Q. Zhang, J. Shi, Y. Li, W. Zhao and J. Shi, *Catal. Commun.*, 2012, **26**, 15–18.
- 6 J. L. Gunjekar, T. W. Kim, H. N. Kim, I. Y. Kim and S.-J. Hwang, *J. Am. Chem. Soc.*, 2011, **133**, 14998–15007.
- 7 F. Wypych, G. A. Bubniak, M. Halma and S. Nakagaki, *J. Colloid Interface Sci.*, 2003, **264**, 203–207; S. Nakagaki, M. Halma, A. Bail, G. G. C. Arizaga and F. Wypych, *J. Colloid Interface Sci.*, 2005, **281**, 417–423.
- 8 S. P. Newman and W. Jones, *New J. Chem.*, 1998, **22**, 105–115; P. G. Cozzi, *Chem. Soc. Rev.*, 2004, **33**, 410–421; S. Bhattacharjee, K.-E. Jeong, S.-Y. Jeong and W.-S. Ahn, *New J. Chem.*, 2010, **34**, 156; E. R. Kleinfeld and G. S. Ferguson, *Science*, 1994, **265**, 370–373; S. W. Keller, H.-N. Kim and T. E. Mallouk, *J. Am. Chem. Soc.*, 1994, **116**, 8817–8818; D. Yan, J. Lu, J. Ma, M. Wei, D. G. Evans and X. Duan, *Angew. Chem., Int. Ed.*, 2011, **50**, 720–723.
- 9 L. Li, R. Z. Ma, Y. Ebina, N. Iyi and T. Sasaki, *Chem. Mater.*, 2005, **17**, 4386–4391; Q. Wu, A. Olafsen, Ø. B. Vistad, J. Roots and P. Norby, *J. Mater. Chem.*, 2005, **15**, 4695; R. Ma, Z. Liu, L. Li, N. Iyi and T. Sasaki, *J. Mater. Chem.*, 2006, **16**, 3809.
- 10 S. Bhattacharjee and J. A. Anderson, *Chem. Commun.*, 2004, 554.
- 11 F. Kooli, I. C. Chisem, M. Vucelic and W. Jones, *Chem. Mater.*, 1996, **8**, 1969–1977.
- 12 M. Meyn, K. Beneke and G. Lagaly, *Inorg. Chem.*, 1990, **29**, 5201–5207.
- 13 S. Bhattacharjee and J. A. Anderson, *Catal. Lett.*, 2004, **95**, 119–125.
- 14 S. Bhattacharjee, *J. Catal.*, 2004, **225**, 398–407.
- 15 J. S. Valente, G. Rodriguez-Gattorno, M. Valle-Orta and E. Torres-Garcia, *Mater. Chem. Phys.*, 2012, **133**, 621–629.
- 16 B. S. Lane, M. Vogt, V. J. DeRose and K. Burgess, *J. Am. Chem. Soc.*, 2002, **124**, 11946–11954; M. Matzapetakis, N. Karligiano, A. Bino, M. Dakanali, C. P. Raptopoulou, V. Tangoulis, A. Terzis, J. Giapintzakis and A. Salifoglou, *Inorg. Chem.*, 2000, **39**, 4044–4051; H. Vezin, E. Lamour, S. Routier, F. Villain, C. Bailly, J. L. Bernier and J. P. Cateau, *J. Inorg. Biochem.*, 2002, **92**, 177–182.